Petrogenesis of Ajil mafic dykes from Eastern Belt of Peninsular Malaysia: fractionated within plate lithospheric mantle magma beneath the eastern Malaya Block

Muhammad Hafifi Badruldin, Azman A. Ghani* and Long Xiang Quek

Department of Geology, Faculty of Sciences,
University of Malaya 50603, Kuala Lumpur, Malaysia

North-eastern trending mafic dykes are found intruding granitic body in Ajil area, Eastern Belt of Peninsular Malaysia. The intrusions display sharp, vertical to sub-vertical contacts to granitic host and consist mainly of plagioclase and clinopyroxene. Majority of the dykes are quartz tholeiite with some olivine tholeiite. All dykes display enrichment in light rare earth elements (LREE) relative to heavy rare earth elements (HREE) and depletion in high field strength elements (HFSE) and Pb. Low compatible elements' content such as MgO, Ni and Cr implied that crystal fractionation were controlled by olivine and clinopyroxene. The dykes were originated from shallow lithospheric mantle, the source region of which has been influenced by hydrous metasomatism. The emplacement of the dykes took place in fault-controlled within-plate tectonic setting.

Keywords: Ajil mafic dykes, clenopyroxene, peninsular Malaysia, petrogenesis, plagioclase.

EASTERN Belt of Peninsular Malaysia (Figure 1) is characterized by extensive Permo-Triassic arc magmatism as a result of Palaeo-Tethys Ocean subduction beneath East Malaya-Indochina Block[1]. The arc magmatism ceased in Late Triassic following the collision of Sibumasu and East Malaya-Indochina blocks. Jurassic–Cretaceous periods in Peninsular Malaysia were mainly controlled by faulting system[2] and major magmatism was absent except for mafic dyke and smaller plutonic intrusions. Hutchison[3] considered this period where Peninsular Malaysia and surrounding region became cratonized. Despite widespread occurrences of the mafic dykes intruding granitic bodies in Eastern Belt, detailed petrogenetic study is yet to exist. This communication reports a new set of geochemical data of mafic dykes from the central part of the Eastern Belt, Peninsular Malaysia.

The study area is located near Ajil town in the state of Terengganu, east of Peninsular Malaysia. The area is made up of Jerangau Forest Pluton (Figure 2). The pluton is further divided into Lerek, Binjai and Payong granites[4]. Lerek and Binjai granites are characterized by pinkish colour, medium- to coarse-grained phaneritic texture. Numerous mafic dykes were intruded and exposed in the western part of Lerek and Binjai granites along 10 km distance from kilometre is 390 to kilometre 400 of East Coast Expressway. Due to the thick tropical vegetation,

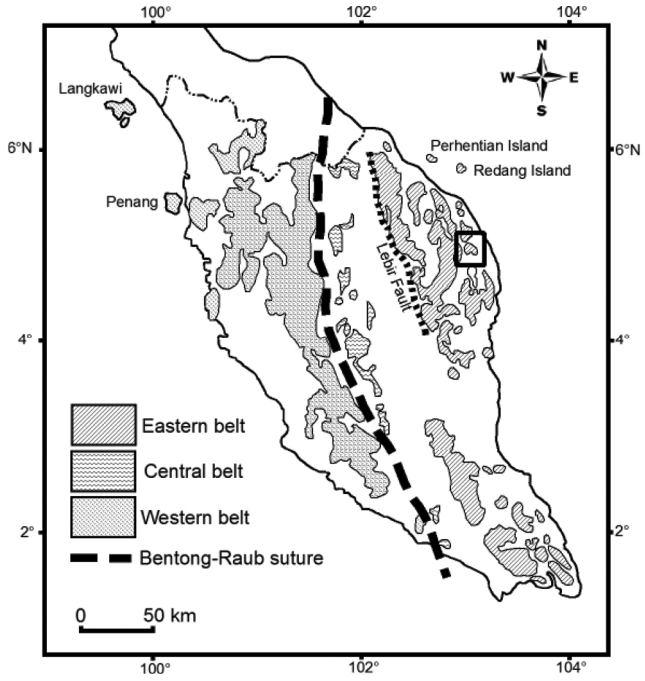

Figure 1. Subdivision of granitic bodies in Peninsular Malaysia[1].

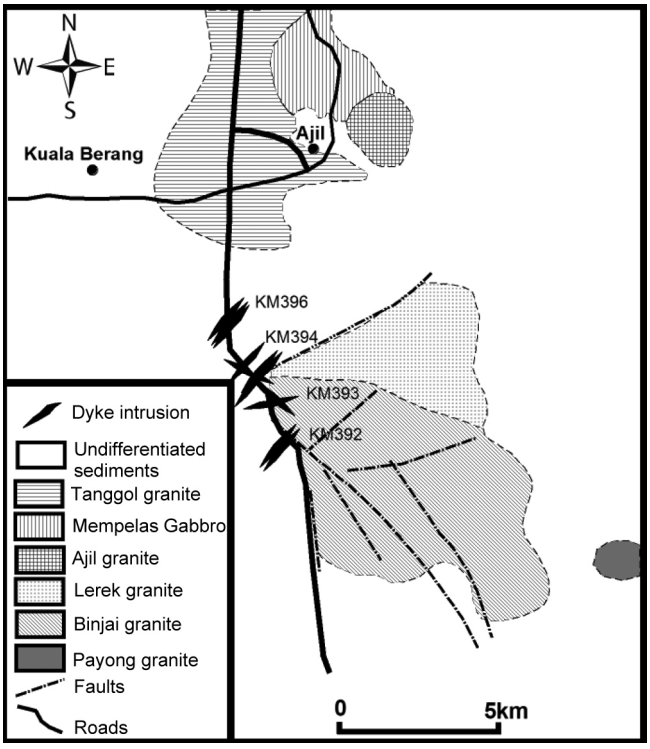

Figure 2. The general geology of the study area near Ajil, Eastern Belt of Peninsular Malaysia[4].

*For correspondence. (e-mail: azmangeo@um.edu.my)

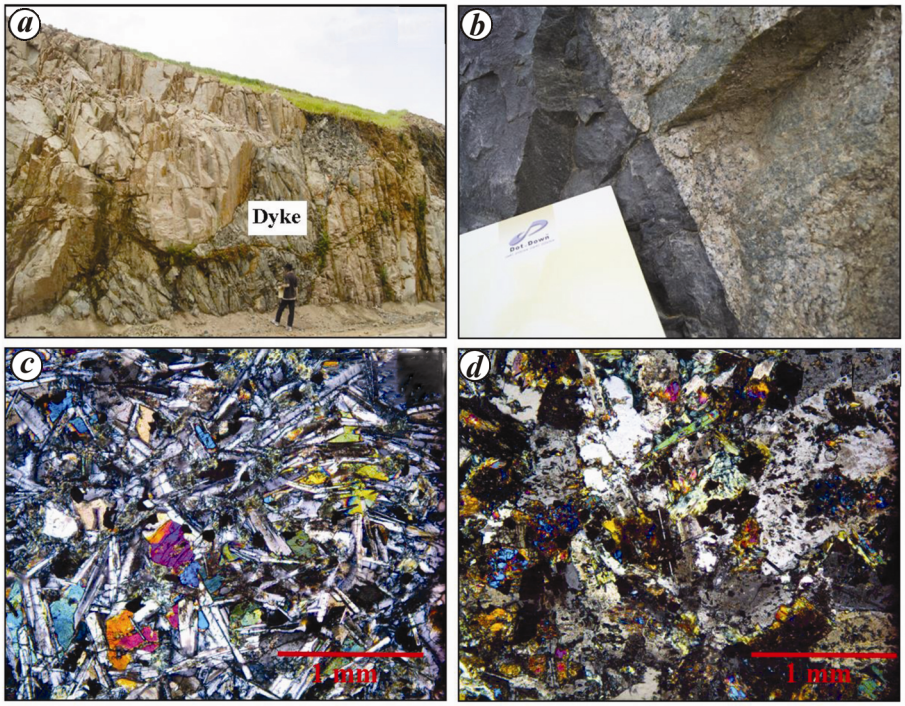

Figure 3. ***a***, Sub-vertical dyke intruding granitic body; ***b***, Dyke displays sharp contact with granitic host; ***c***, Subophitic and doleritic texture with prismatic lath-shaped plagioclase and subhedral clinopyroxene; ***d***, Medium-grained, subhedral to anhedral plagioclase enclosing clinopyroxene crystals.

the dyke intrusions cannot be traced throughout the pluton.

The dykes are dark grey in colour and occur as fine- to medium-grained, aphanitic to micro-porphyritic textures. The widths of the dykes range from several centimetres to more than 10 m and have sharp, vertical to sub-vertical contacts with the granitic host (Figure 3 *a*, *b*). They strike NE–SW and some dykes show NW–SE trending. Their trends are different from the trends of dykes in northern (N–S trending in Perhentian Island) and southern (E–W trending in Kuantan district) parts of the study area[5]. The occurrence of chilled margin inside one dyke body displays a feature of composite dyke and suggests multi-episodic intrusion in this area.

In thin section, the dykes show fine- to medium-grained, intergranular, subophitic and doleritic textures and consist of plagioclase and clinopyroxene as its dominant minerals with minor quantities of epidote, hornblende and opaque minerals (Figure 3 *c*, *d*). Secondary minerals are sericite and chlorite. Plagioclase occurs as long, prismatic lath-shaped, euhedral to subhedral grains and shows well-developed twinning. Clinopyroxene occurs as fine- to medium-grained, subhedral to anhedral intergranular grains and sometimes occurs as subophitic and interstitial to plagioclase. Opaque minerals are abundant. In some samples, phenocrysts of plagioclase and clinopyroxene are also present.

Twenty-three representative samples have been analysed for major and trace elements at ACME Labs, Vancouver, Canada. Major elements were determined using X-ray fluorescence spectrometry (XRF) whereas trace elements were determined using inductively coupled plasma mass spectrometry (ICP-MS) with internal reference materials. The geochemical data obtained is presented in Table 1.

Overall, the dykes have variable SiO_2 (43.1–56.8%), Al_2O_3 (13.97–19.14%), CaO (0.85–10.54%), $Fe_2O_3^t$ (8.09–17.2%), MgO (3.03–8.98%), Na_2O (1.80–6.38%), K_2O (0.39–2.27%), MnO (0.12–0.80%), TiO_2 (1.03–3.12%) and P_2O_5 (0.17–0.98%) with Mg# ranging from 31.4–57.7 {Mg# = 100*(MgO/40.32)/[(MgO/40.32) + (FeO/71.85)]}. Selected trace elements contents are Zr (83.8–356.7 ppm), Ni (1.1–137.7 ppm), Co (18.6–46.5 ppm), Cr (41–369 ppm), Ba (24–660 ppm) and Sr (106.4–690.1 ppm). The dykes exhibit positive correlations between Al_2O_3, Ni and Cr and negative correlations between Fe_2O_3, TiO_2, P_2O_5, Zr and Y against Mg# in variation diagrams (Figure 4).

In total alkali-silica (TAS) diagram (Figure 5 *a*), most of the dykes display transitional alkaline affinity. However, CIPW calculation shows 20 samples are quartz normative and 3 samples (DY2, DY6 and DY14) are olivine normative. All dykes are plotted within quartz tholeiite except DY2, DY6 and DY14 which are plotted within olivine tholeiite fields in Q-Hy-Di-Ol-Ne diagram[6] (Figure 5 *b*). Since normative nepheline is absent, the studied dykes cannot be considered as alkaline. Because alkalis are mobile during alteration, immobile elements

Table 1. Major and trace elements analyses of the mafic dykes from Ajil areas

Sample	DY1	DY2	DY3	DY4	DY5	DY6	DY7	DY8	DY9
Major elements (wt%)									
SiO_2	56.8	49.1	51.3	53.5	50	49.9	50.2	51.2	52.3
Al_2O_3	14.93	15.01	16.31	15.05	16.01	15.38	17	17.29	14.22
$Fe_2O_3^t$	9.65	13.12	11.8	11.57	10.72	12.01	11.92	11.91	11.34
CaO	4.1	7.35	1.29	3.83	6.85	7.2	4.05	1.44	5.3
MgO	3.03	4.18	6.69	3.41	6.59	4.95	4.91	4.55	4.27
Na_2O	5.42	5.23	5.12	6.38	3.79	4.85	3.38	3.1	5.34
K_2O	1.78	0.54	1.02	0.86	1.36	0.96	1.28	2.2	1.34
MnO	0.17	0.24	0.26	0.26	0.19	0.24	0.13	0.12	0.26
TiO_2	1.78	2.63	1.94	2.6	1.47	1.98	2.23	2.21	2.11
P_2O_5	0.52	0.56	0.39	0.98	0.29	0.4	0.78	0.79	0.37
Cr_2O_3	0.01	0.013	0.014	0.006	0.024	0.017	0.009	0.011	0.021
LOI	2.04	2.5	4.5	2.11	3.21	2.86	4.73	5.36	2.5
Total	100.27	100.48	100.67	100.54	100.48	100.72	100.61	100.16	99.41
Mg#	38.31	38.66	52.86	36.83	54.87	44.91	44.90	43.04	42.69
Trace elements (ppm)									
Ba	266	74	166	116	261	125	275	280	151
Be	3	1	4	3	<1	7	3	2	4
Co	18.6	33.6	35.2	19.1	34.4	32	30.9	29.6	26.6
Cs	0.3	0.1	1.9	0.2	0.6	0.2	1.8	2.7	0.3
Ga	21.1	20.8	21.1	20.8	16.9	17.9	19.6	20.8	19.4
Hf	8.3	6.4	5	7.5	4.5	4.7	6.7	8.1	8.2
Nb	16.1	10.3	8.2	11.5	9.2	9.2	22.8	25	14
Rb	49.1	15	41.4	23.6	64.2	26.2	55.5	137	36.2
Sn	4	3	2	4	2	1	2	2	3
Sr	264.2	228.8	236.3	212.9	410.7	176.1	606.4	294.1	144
Ta	0.9	0.7	0.6	0.9	0.6	0.5	1.3	1.4	1.1
Th	6.1	2.1	2.9	3.1	3.9	2	3.6	4.3	3.9
U	1.6	0.5	0.8	0.8	1	0.5	1.7	1.4	1.1
V	185	353	296	192	169	301	219	214	249
W	0.7	0.8	1.1	0.5	1.2	1.6	<0.5	1.5	1
Zr	356.7	252.1	202.8	289.7	170.6	191.6	302.3	330.2	332.1
Y	57.4	50.9	38.9	59.1	32.7	34.6	38	45.5	49.7
La	37.3	23.7	18	33.1	24.1	18.2	50.1	55.1	26.3
Ce	88.7	62.4	43.4	81.7	55.4	46.7	109	121.9	66
Pr	10.77	8.07	5.76	10.8	6.21	6.13	12.28	13.84	8.35
Nd	46.5	36.6	25.9	48.1	25.1	30	48.1	57.6	37.5
Sm	10.23	9.14	6.38	11.32	5.88	6.59	9	10.3	8.59
Eu	2.66	2.92	1.85	3.42	1.77	1.92	2.36	2.58	2.28
Gd	10.73	9.83	6.77	11.44	5.7	6.94	8.55	9.72	8.87
Tb	1.71	1.65	1.11	1.88	0.98	1.14	1.28	1.44	1.56
Dy	10.32	9.76	6.81	11.41	6.49	6.65	7.03	8.49	8.62
Ho	2.24	1.95	1.44	2.21	1.27	1.44	1.46	1.8	2.05
Er	6.64	5.63	4.34	6.41	3.82	3.95	4.12	4.78	5.74
Tm	0.94	0.75	0.57	0.89	0.59	0.58	0.56	0.64	0.91
Yb	6.24	4.61	3.58	5.59	3.64	3.49	3.77	4.14	5.53
Lu	0.91	0.85	0.59	0.82	0.58	0.57	0.56	0.7	0.85
Mo	1.5	0.9	0.5	1	0.9	0.7	0.7	1	1.5
Cu	9.3	21.3	22	6.9	43.1	30.2	18.7	20.7	29
Pb	2	3.3	3.3	2.2	1.7	5.9	2.1	7	2.2
Zn	88	95	109	90	65	86	125	189	82
Ni	5.4	10	39.4	1.1	89.3	14.9	24	22.3	18.4
Cr	68	89	96	41	164	116	62	75	144

Sample	DY10	DY12	DY13	DY14	DY15	DY17	DY18
Major elements (wt%)							
SiO_2	46.2	46.7	46.9	49.3	48.8	56.1	47.9
Al_2O_3	16.66	17.67	16.66	14.71	14.47	15.51	16.62
$Fe_2O_3^t$	17.2	15.38	8.32	12.3	12.27	8.09	10.74
CaO	1.51	0.85	8.53	7.99	9.05	6.08	10.02

(*Contd*)

Table 1. (*Contd*)

Sample	DY10	DY12	DY13	DY14	DY15	DY17	DY18
MgO	4.41	5.8	6.36	5.44	5.18	4.86	7.06
Na_2O	3.5	3.29	2.00	4.56	3.53	3.74	2.67
K_2O	0.73	1.14	2.05	0.95	0.72	1.32	0.67
MnO	0.19	0.22	0.14	0.22	0.21	0.16	0.19
TiO_2	3.12	2.73	1.13	2.22	2.17	1.03	1.47
P_2O_5	0.87	0.47	0.34	0.44	0.41	0.25	0.38
Cr_2O_3	0.016	0.017	0.015	0.021	0.023	0.031	0.03
LOI	5.82	6.18	7.56	2.31	2.73	3.04	2.82
Total	100.19	100.51	100.01	100.5	99.56	100.23	100.53
Mg#	33.65	42.72	60.19	46.66	45.51	54.30	56.53
Trace elements (ppm)							
Ba	24	73	337	373	117	356	177
Be	5	3	4	<1	2	3	<1
Co	39.2	36.8	29.2	30.9	32.3	25.4	35.5
Cs	2.2	2.0	5.7	0.6	1.4	0.5	1.2
Ga	22.4	24.0	14.5	16.2	18.4	16.3	15.7
Hf	5.5	5.7	2.5	4.5	5.1	4.3	4.5
Nb	9.4	9.9	9.0	7.4	8.7	9.5	10.3
Rb	51.6	66.4	104.5	31.4	27.5	48.1	32.8
Sn	2	2	<1	2	2	1	1
Sr	106.4	120.8	638.6	683.5	540.8	497.0	494.5
Ta	0.7	0.7	0.6	0.6	0.5	0.7	0.6
Th	1.4	1.7	2.9	1.6	1.7	7.0	1.6
U	1.1	0.7	0.8	0.4	0.4	1.7	0.5
V	334	283	152	286	293	117	193
W	15.2	3.1	<0.5	<0.5	<0.5	0.6	0.6
Zr	228.3	220.5	115.3	207.1	200.0	199.0	197.5
Y	70.8	35.8	19.2	37.6	38.3	29.1	31.3
La	24.5	17.6	22.9	17.7	17.6	31.3	27.0
Ce	60.3	48.4	49.9	43.7	45.4	64.7	62.3
Pr	7.66	6.37	5.47	5.92	6.13	7.3	7.04
Nd	34.7	27.7	22.8	25.5	28.0	26.1	28.9
Sm	8.49	6.94	4.18	6.24	6.48	5.53	5.85
Eu	2.45	1.71	1.36	1.93	1.99	1.30	1.60
Gd	9.77	6.36	4.22	7.07	6.75	5.40	5.52
Tb	1.72	0.99	0.65	1.14	1.16	0.82	0.93
Dy	11.33	5.75	3.68	7.05	6.90	4.65	5.72
Ho	2.44	1.32	0.73	1.53	1.57	1.10	1.21
Er	7.21	3.88	1.84	4.38	4.28	3.09	3.38
Tm	1.05	0.62	0.29	0.53	0.59	0.43	0.51
Yb	6.25	3.87	2.03	3.39	3.92	2.72	3.06
Lu	1.03	0.64	0.30	0.57	0.62	0.46	0.53
Mo	0.8	0.3	0.6	0.8	0.8	0.9	0.8
Cu	0.7	0.7	24.0	39.3	33.7	25.1	37.8
Pb	3.2	1.0	1.8	2.7	2.1	2.9	2.1
Zn	177	239	49	71	78	56	51
Ni	29.4	53.4	59.7	15.7	16.1	43.5	75.8
Cr	109	116	103	144	157	212	205

Sample	DY20	DY21	DY22	DY23	DY25	DY26	DY27
Major elements (wt%)							
SiO_2	47.9	48.8	50.2	47.9	48.3	47.4	45.1
Al_2O_3	14.78	13.97	14.15	14.04	15.86	17.33	16.19
$Fe_2O_3^t$	13.37	13.71	13.29	12.58	11.35	12.54	9.68
CaO	8.47	8.4	6.94	8.57	8.81	2.47	9.94
MgO	5.01	5.02	4.1	5.46	7	6.05	6.51
Na_2O	3.67	4.55	4.4	4.26	2.73	2.1	1.8
K2O	0.75	0.39	0.87	0.5	0.73	0.72	1.84
MnO	0.23	0.23	0.22	0.21	0.18	0.2	0.17
TiO_2	3.03	2.72	2.7	2.34	1.88	2.1	1.22

(*Contd*)

Table 1. (*Contd*)

Sample	DY20	DY21	DY22	DY23	DY25	DY26	DY27
P_2O_5	0.54	0.5	0.6	0.46	0.56	0.62	0.34
Cr_2O_3	0.017	0.011	0.01	0.02	0.033	0.029	0.028
LOI	2.76	2.32	2.5	3.67	2.63	8.44	7.19
Total	100.53	100.61	99.96	100.07	100.05	99.99	100.01
Mg#	42.57	42.00	37.90	46.19	54.95	48.83	57.07
Trace elements (ppm)							
Ba	116	103	196	151	173	158	246
Be	3	3	1	1	<1	9	<1
Co	32.4	35.3	28.3	34.9	34.6	39.1	36.5
Cs	0.3	0.2	0.3	0.3	1.1	2.2	5.7
Ga	20.8	17.9	19.3	17.9	17	18.9	13.3
Hf	6.7	5.6	5.3	4.4	2.9	5.1	2.3
Nb	11.9	8.8	10	8.3	12.9	16.7	7.8
Rb	19.6	10.8	20.6	19.4	31.6	43.9	116.8
Sn	2	2	2	2	3	2	<1
Sr	303.9	334.4	346.7	480.5	519.3	276.8	423.7
Ta	0.8	0.6	0.6	0.5	0.8	1	0.5
Th	2.2	1.9	3.1	1.8	4.7	2.4	1.3
U	0.5	0.4	0.7	0.5	1.2	0.6	0.3
V	326	356	307	312	194	223	177
W	2.5	0.6	1.1	<0.5	1	3.6	2.1
Zr	246.6	224.4	243.3	218.7	100.7	211	103.2
Y	43.1	41.8	46.4	37.2	29.4	30.9	21.4
La	23	20.4	23.6	18.4	24.1	35.4	18.9
Ce	58	52.6	61.9	46.7	56.3	79.3	42.4
Pr	7.34	6.7	7.84	6.05	7.08	9.28	4.89
Nd	38	31.6	36.5	28	29.1	33.7	21.9
Sm	8.22	7.06	8.36	6.43	6.45	7.3	3.96
Eu	2.47	2.34	2.47	2.04	1.76	2.01	1.31
Gd	8.22	8.19	8.55	7	6.4	6.65	3.97
Tb	1.33	1.28	1.42	1.19	0.99	1.01	0.65
Dy	8.27	7.86	7.8	6.91	5.27	5.66	3.46
Ho	1.78	1.68	1.83	1.52	1.21	1.16	0.86
Er	5.11	4.48	5.13	4.13	3.44	3.28	2.1
Tm	0.66	0.64	0.7	0.55	0.41	0.48	0.31
Yb	4.14	3.77	4.15	3.3	2.72	2.88	1.98
Lu	0.67	0.59	0.72	0.56	0.44	0.45	0.33
Mo	0.9	1.1	1.2	0.8	0.7	0.7	0.4
Cu	18.3	26.9	11.7	26.1	30.9	29.3	38.4
Pb	1.6	1.3	2.5	1.2	2.4	2	4
Zn	99	87	86	74	48	78	55
Ni	12.6	11.3	7	27.4	74.6	93.6	90.7
Cr	116	75	68	137	226	198	192

ratios may be more reliable to determine their magmatic affinity. Low Nb/Y (0.13–0.60) ratios (Nb/Y<0.5) and negative trend in TiO_2 versus Mg# variation diagram also display a typical tholeiitic affinity[7]. Thus the dykes are considered to be as tholeiitic subalkaline affinity.

The dykes exhibit LREE enrichment relative to HREE in chondrite-normalized diagram (Figure 5 *c*) with moderate to high La_N/Yb_N (2.64–8.97) and La_N/Sm_N (1.60–3.56) ratios, suggesting an enriched mantle source[8]. The absent of strong HREE depletion suggests the absence of residual garnet in the source[9]. The total REE (∑REE) values are 107.02–293.03. In primitive mantle-normalized multi-element variation diagram[10] (Figure 5 *d*), the dykes display notable HFSE and Pb depletion with elevated Th, U and La.

The role of olivine and clinopyroxene fractionations is shown by their low content of compatible elements such as MgO (3.03–7.06%), Ni (1.1–93.6 ppm), Co (18.6–39.2 ppm) and Cr (41–226 ppm) as well as Mg# (31.36–57.67). In Ti versus Zr diagram (Figure 6 *b*), the dykes display distinct concave downward pattern implying changes in fractionation phases. Fractionation of olivine and clinopyroxene increase both Ti and Zr concentrations whereas magnetite fractionation will decrease Ti but not Zr. Lack of significant Eu negative anomaly (Eu/Eu*: $Eu_N/\sqrt{(Sm_N) \cdot (Gd)_N)}$ = 0.73–1.01) suggests plagioclase fractionation is insignificant.

It is important to evaluate whether the dykes were formed in a continental intra-plate or arc-related settings. Continental intra-plate basalts generally contain high Zr

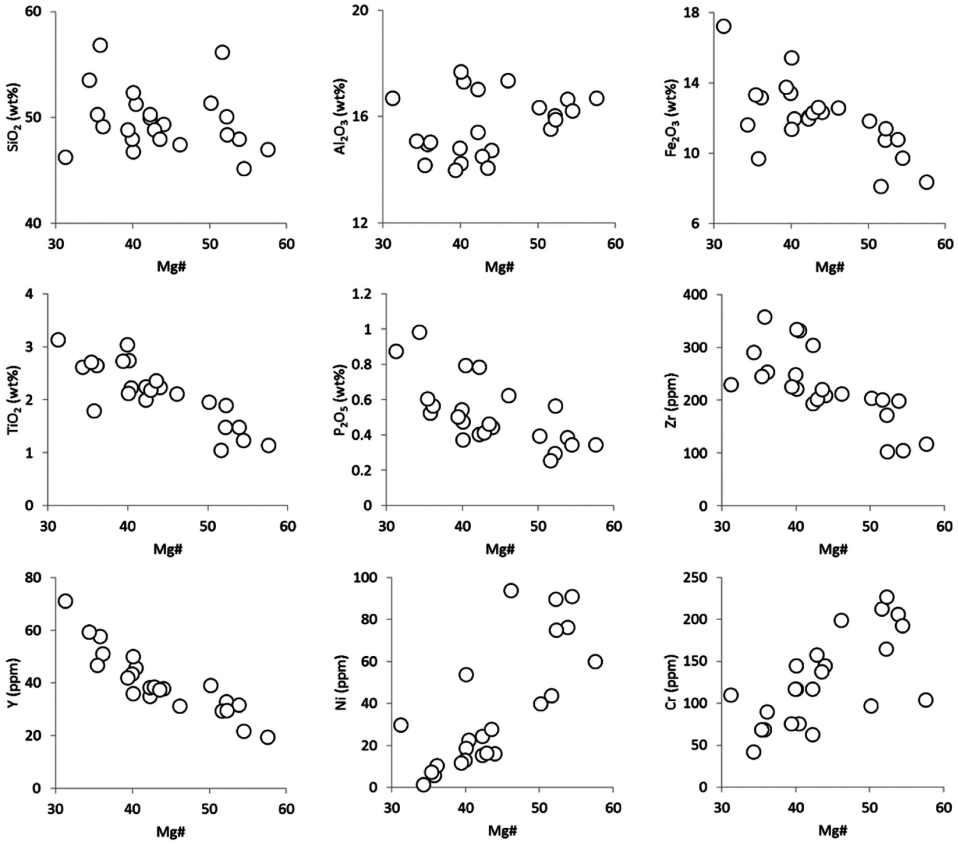

Figure 4. Variation diagrams of selected major and trace elements versus Mg# for the mafic dykes from Ajil, Eastern Belt of Peninsular Malaysia.

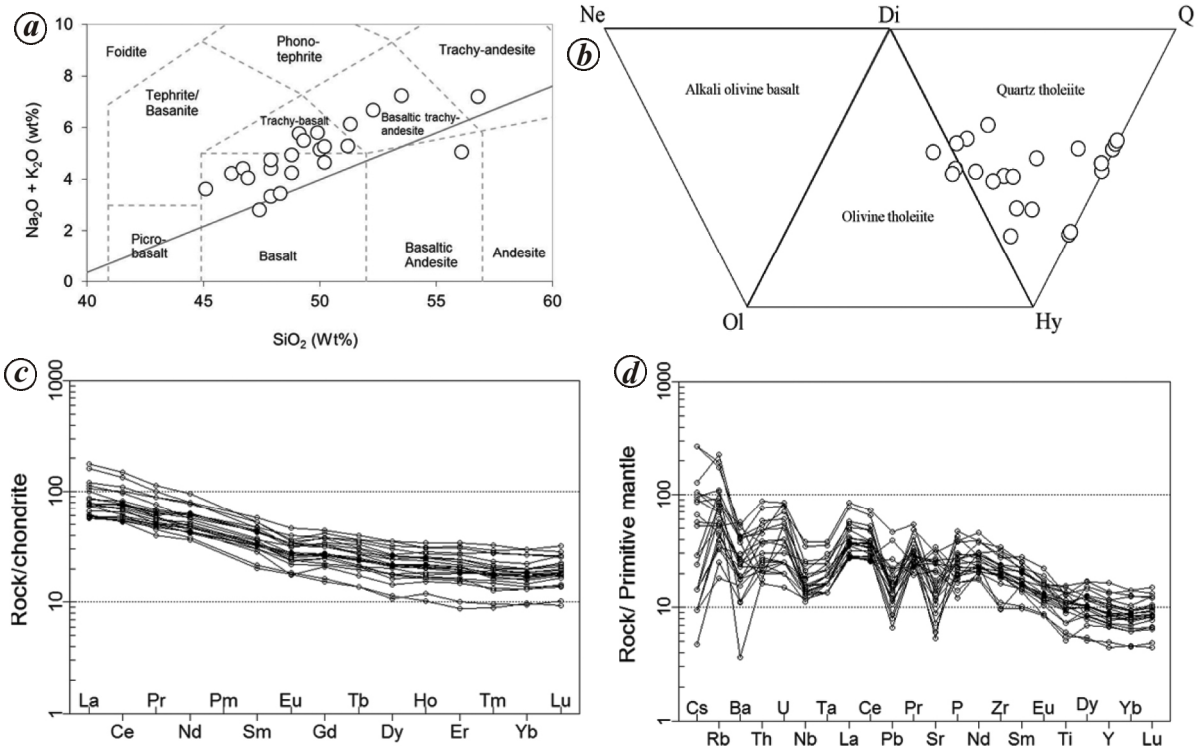

Figure 5. ***a***, The dykes display transitional affinity in TAS classification diagram; ***b***, Most of the dykes are plotted on quart tholeiite field except three samples are plotted on olivine tholeiite field in normative diagram; ***c***, LREE enrichment relative to HREE in chondrite-normalized diagram; ***d***, The dykes display notable HFSE and Pb depletion in primitive mantle-normalized diagram.

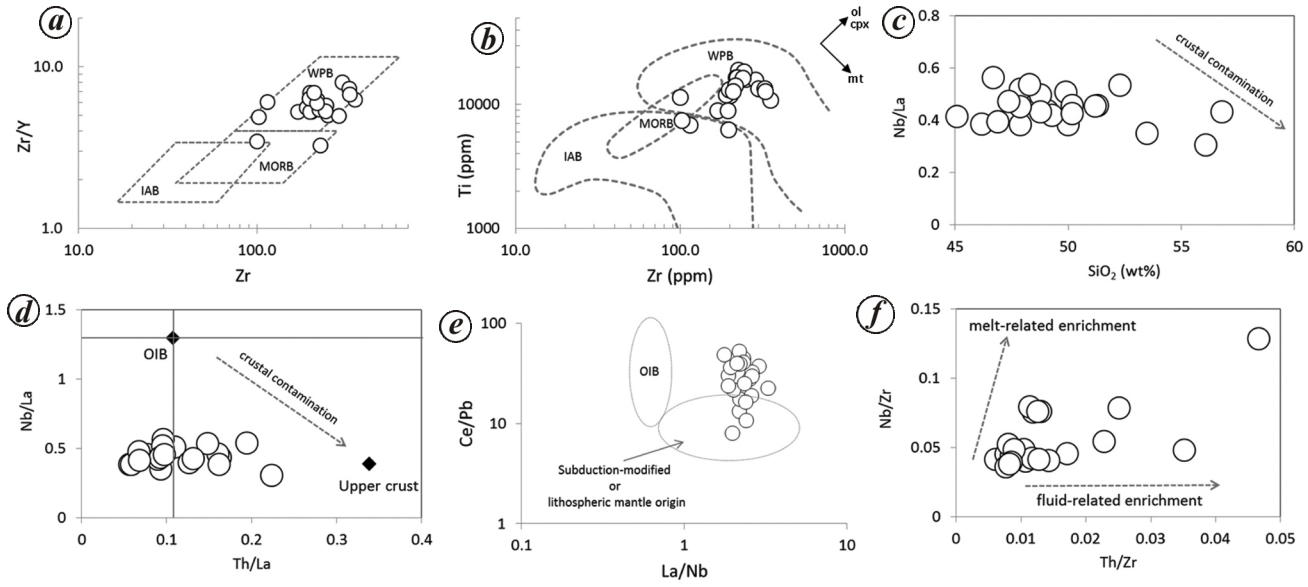

Figure 6. ***a***, Most of the dykes are plotted on within-plate basalt (WPB) field in Zr/Y versus Zr diagram; ***b***, Most of the dykes are plotted on WPB field in Ti versus Zr diagram; ***c***, Nb/La versus SiO_2 diagram displays relatively horizontal trend in contrast to crustal contamination (negative) trend; ***d***, Nb/La versus Th/La diagram displays relatively horizontal trend in contrast to crustal contamination (negative) trend; ***e***, The studied dykes are plotted on subduction-modified/lithospheric mantle origin field in Ce/Pb versus La/Nb diagram; ***f***, The dykes show fluid-related enrichment in Nb/Zr versus Th/Zr diagram.

(>70 ppm)[11] content, Zr/Y (>3.4)[11], Zr/Sm (≈30)[12] and Ti/V (20–50)[13] ratios. On the contrary, arc-related basalts contain low Zr (<130 ppm)[11] content, Zr/Y (<3.3)[11], Zr/Sm (<20)[12] and Ti/V (<20)[13] ratios. The studied dykes have high Zr (100.7–356.7 ppm) contents, Zr/Y (3.22–7.96), Zr/Sm (15.6–38.7) and Ti/V (39.3–81.2) ratios, compared to continental intra-plate basalts. In Zr/Y versus Zr diagram[14] (Figure 6 *a*), all dykes are plotted on WPB field except for DY10 and DY25 plotted on MORB field. In Ti versus Zr diagram[15] (Figure 6 *b*), most of the dykes are plotted on Within Plate Basalt (WPB) field except for DY25 plotted on MORB-WPB field and DY13, DY17 and DY27 plotted on Island Arc Basalt (IAB) field. The transitional MORB-within plate feature suggests an initial stage of continental rifting[15]. Field observation also shows the studied dykes crosscut Permo-Triassic arc-related granite, suggesting that their emplacement took place during post-crystallization of granite.

Depletion in HFSE and low Nb/La (0.30–0.56) ratios indicate crustal contamination[11]. In Nb/La versus SiO_2 plot, the dykes show relative horizontal trend (Figure 6 *c*). In Nb/La versus Th/La plot (Figure 6 *d*), the dykes are plotted near the Th/La ≈ OIB (Oceanic Island Basalt)[16] line and away from the upper crust[17]. Crustal contamination displays negative correlation in both diagrams. Furthermore, some researchers[18–20] argue that HFSE depletion and Nb/La ratio are more sensitive to hydrous metasomatism. Thus, we imply that HFSE depletion and low Nb/La ratio reflect their mantle source characteristics rather than crustal contamination.

Earlier researchers[5,21] suggest dyke emplacement occurred as a result of mantle upwelling. Hutchison[21] explained that mantle upwelling beneath South China Sea caused crustal fracturing during Cretaceous period which was later filled with the mafic magma. Ghani *et al.*[5] suggested a slab break-off model, where the rising asthenospheric magma intruded through fractures in relatively thinner East Malaya crust. The dykes studied do not show strong HREE depletion with moderate La_N/Yb_N (2.64–8.97), Gd_N/Yb_N (1.26–1.90) and Dy_N/Yb_N (0.96–1.37) ratios, suggesting a shallow lithospheric mantle origin[9]. Hence, the magma source for dykes from Ajil is of plume-related origin since mantle plume requires deeper source in the upper mantle[22].

Potential candidate for the mantle source region of the studied dykes is from sub-continental lithospheric mantle (SCLM). The dykes have relatively high La/Nb (1.78–3.29), La/Ta (23.9–45.0) and Zr/Nb (7.8–28.0) ratios. These values suggest that SCLM source region has been influenced by hydrous metasomatism[23–26]. In Ce/Pb versus La/Nb diagram[23] (Figure 6 *e*), the dykes are plotted on subduction-related (influenced by metasomatism) or lithospheric mantle origin field. The influence of hydrous metasomatism in their mantle source region[27–30] is further supported by subchondritic Nb/Ta (12.3–18.4), superchondritic Zr/Hf (34.7–49.7) and also Th/Zr enrichment relative to Nb/Zr in Nb/Zr versus Th/Zr diagram[30] (Figure 6 *f*).

However, what causes hydrous metasomatism to the source region of dykes is unknown due to the lack of geochronology and isotopic data. Whether their magma was a product of partial melting of SCLM due to direct slab dehydration or partial melting of metasomatic veins in the lithospheric mantle during post-subduction period,

remains speculative. Another question that arises in this study is, what mechanisms are involved in triggering the mafic dykes magmatism during Jurassic to Cretaceous periods? These are important aspects which require further investigation.

A new detailed geochemical data of mafic dykes from Ajil in Eastern Belt of Peninsular Malaysia is presented here. The outcome of the present study is: (1) the dykes are considered as tholeiitic subalkaline affinity; (2) fractionating phases are mainly controlled by olivine and clinopyroxene; (3) the dykes were emplaced in fault-controlled within-plate setting; (4) the dykes originated from shallow lithospheric mantle and their source region has been influenced by fluid-related metasomatism.

1. Searle, M. P. *et al.*, Tectonic evolution of the Sibumasu-Indochina terrane collision zone in Thailand and Malaysia: constraints from new U-Pb zircon chronology of SE Asian tin granitoids. *J. Geol. Soc.*, 2012, **169**, 489–500.
2. Tjia, H. D. and Gobbett, D. J., Tectonic history. In *Geology of the Malay Peninsula: West Malaysia and Singapore* (eds Gobbett, D. J. and Hutchison, C. S.), John Wiley-Interscience, New York, 1973, pp. 305–330.
3. Hutchison, C. S., Tectonic evolution of Sundaland: a Phanerozoic Synthesis. *Bull. Geol. Soc. Malaysia*, 1973, **6**, 61–86.
4. Cobbing, E. J., Pitfield, P. E. J., Darbyshire, D. P. F. and Mallick, D. I. J., The granites of the South-East Asian Tin Belt. Overseas Memoir 10. British Geological Survey, 1992.
5. Ghani, A. A., Lo, C.-H. and Chung, S.-L., Basaltic dykes of the Eastern Belt of Peninsular Malaysia: the effects of the difference in crustal thickness of Sibumasu and Indochina. *J. Asian Earth Sci.*, 2013, **77**, 127–139.
6. Thompson, R. N., Dispatches from the basalt front. 1. Experiments. *Proc. Geol. Ass.*, 1984, **95**, 249–262.
7. Winchester, J. A. and Floyd, P. A., Geochemical discrimination of different magma series and their differentiation products using immobile elements. *Chem. Geol.*, 1977, **20**, 325–343.
8. Hooper, P. R. and Hawkesworth, C. J., Isotopic and geochemical constraints on the origin and evolution of the Columbia River basalt. *J. Petrol.*, 1993, **34**, 1203–1246.
9. Blundy, J. D., Robinson, J. A. C. and Wood, B. J., Heavy REE are compatible in clinopyroxene on the spinel lherzolite solidus. *Earth Planet. Sci. Lett.*, 1998, **160**, 493–504.
10. McDonough, W. F. and Sun, S. S., Composition of the Earth. *Chem. Geol.*, 1995, **120**, 223–253.
11. Xia, L. Q., The geochemical criteria to distinguish continental basalts from arc related ones. *Earth Sci. Rev.*, 2014, **139**, 195–212.
12. Wilson, M., *Igneous petrogenesis*. Unwin Hyman, London, UK, 1989, p. 466.
13. Shervais, J. W., Ti–V plots and the petrogenesis of modern and ophiolitic lavas. *Earth Planet. Sci. Lett.*, 1982, **59**, 101–118.
14. Pearce, J. A. and Norry, M. J., Petrogenetic implications of Ti, Zr, Y, and Nb variations in volcanic rocks. *Contrib. Mineral. Petrol.*, 1979, **69**, 33–37.
15. Pearce, J. A., Trace element characteristics of lavas from destructive plate boundaries. In *Andesites* (ed. Thrope, R. S.), Wiley, New York, 1982, pp. 525–548.
16. Sun, S. S. and McDonough, W. F., Chemical and isotopic systematic of oceanic basalts: implications for mantle composition and processes. In *Magmatism in the Ocean Basins* (eds Saunders, A. D. and Norry, M. J.), Geological Society Special Publication, 1989, vol. 42, 313–345.
17. Rudnick, R. L. and Gao, S., *Composition of the Continental Crust. Treatise on Geochemistry*, Elsevier, Amsterdam, 2003, **3**, 1–64.
18. Hawkesworth, C. J., Lightfoot, P. C., Fedorenko, V. A., Blake, S., Naldrett, A. J., Doherty, W. and Gorbachev, N. S., Magma differentiation and mineralisation in the Siberian continental flood basalts. *Lithos*, 1995, **34**, 61–88.
19. Puffer, J. H., Contrasting high field strength element contents of continental flood basalts from plume versus reactivated-arc sources. *Geology*, 2001, **29**, 675–678.
20. Murphy, J. B. and Dostal, J., Continental mafic magmatism of different ages in the same terrane: constraints on the evolution of an enriched mantle source. *Geology*, 2007, **35**, 335–338.
21. Hutchison, C. S., *Geological Evolution of South-East Asia*, Geological Society of Malaysia, Malaysia, 2007, 2nd edn.
22. Morgan, W. J., Convection plumes in the lower mantle. *Nature*, 1971, **230**, 42–43.
23. Fitton, J. G., Coupled molybdenum and niobium depletion in continental basalts. *Earth Planet. Sci. Lett.*, 1995, **136**, 715–721.
24. Gibson, S. A., Thompson, R. N., Leonardos, O. H., Dickin, A. P. and Mitchell, J. G., The limited extent of plume–lithosphere interactions during continental flood-basalt genesis: geochemical evidence from Cretaceous magmatism in southern Brazil. *Contrib. Mineral. Petrol.*, 1999, **137**, 147–169.
25. Le Roex, A. P., Dick, H. J. B., Erlank, A. J., Reid, A. M., Frey, F. A. and Hart, S. R., Geochemistry, mineralogy and petrogenesis of lavas erupted along the south west Indian ridge between the Bouvet triple junction and 11 degrees east. *J. Petrol.*, 1983, **24**, 267–318.
26. Thompson, R. N. and Morrison, M. A., Asthenospheric and lower-lithospheric mantle contributions to continental extension magmatism: an example from the British Tertiary Province. *Chem. Geol.*, 1988, **68**, 1–15.
27. Dupuy, C., Liotard, J. M. and Dostal, J., Zr/Hf fractionation in intraplate basaltic rocks: carbonate metasomatism in the mantle source. *Geochim. Cosmochim. Acta*, 1992, **56**, 2417–2423.
28. Jörg, A., Pfänder, J. A., Münker, C., Stracke, A. and Mezger, K., Nb/Ta and Zr/Hf in ocean island basalts – implications for crust-mantle differentiation and the fate of Niobium. *Earth Planet. Sci. Lett.*, 2007, **254**, 158–172.
29. Chen, Y. *et al.*, Slab breakoff triggered ca. 113 Ma magmatism around Xainza area of the Lhasa Terrane, *Tibet. Gondwana Res.*, 2014, **26**(2), 449–463.
30. Kepezhinskas, P., McDermott, F., Defant, M. J., Hochstaedter, A. and Drummond, M. S., Trace element and Sr–Nd–Pb isotopic constraints on a three-component model of Kamchatka Arc petrogenesis. *Geochim. Cosmochim. Acta*, 1997, **61**, 577–600.

ACKNOWLEDGEMENTS. This work was partly supported by the University of Malaya (UMRG Grant No. RG263/13AFR) and UM/MOHE High Impact Research Grant (UMC/HIR/MOHE/SC/27).

Received 2 February 2016; revised accepted 26 April 2017

doi: 10.18520/cs/v113/i07/1448-1455